


ORIGINAL RESEARCH

Intelligent islanding detection in smart microgrids using variance autocorrelation function-based modal current envelope

Shanzah Naseem¹ | Sadiq Ahmad¹ | Saddam Aziz² | Muhammad Ali² |
Kazi N. Hasan³  | Ayaz Ahmad^{1,4} | Abdullah Shoukat⁵

¹Department of Electrical & Computer Engineering, COMSATS University Islamabad, Islamabad, Pakistan

²Department of Electrical and Electronic Engineering, The Hong Kong Polytechnic University, Hung Hom, Hong Kong

³School of Engineering, RMIT University, Melbourne, Victoria, Australia

⁴Department of Electrical Engineering, College of Engineering, King Faisal University, Al-Ahsa, Saudi Arabia

⁵Department of Precision Machinery and Instruments, School of Engineering Science, University of Science and Technology of China, Anhui, China

Correspondence

Kazi N. Hasan.
Email: kazi.hasan@rmit.edu.au

Abstract

Islanding detection is a critical issue in grid-connected distributed microgrid systems. Distributed generation in the current power system has caused many challenges. Consequently, detecting quick and effective islanding is the most critical issue to minimise equipment failure, avoid danger, and maintain grid safety. There are various techniques for islanding identification in microgrids. Three classifications have been applied to categorise these strategies, which are: active, passive, and hybrid. This paper proposes and demonstrates an efficient and accurate approach to islanding detection based on the Variance Autocorrelation Function of a Modal Current Envelope (VAMCE) technique. Demodulation techniques including synchronous real demodulation, square law demodulation, asynchronous complex square law demodulation, and the quadrature demodulation technique are employed to detect the envelope of the 3-phase current signal. The VAMCE methodology is better suited for islanding detection because of its response to current sensitivity under islanding scenarios but not under normal conditions. Several simulations under various settings, including normal and islanded scenarios are used to analyse this method. These simulations have demonstrated different situations, such as when the system works normally and when it does not. The VAMCE along with the quadrature demodulation technique outperforms the others. The proposed solution is not only more accurate but also much faster compared to other methods. The proposed approach can identify normal and islanded situations in just 0.4 s.

KEYWORDS

fault diagnosis, microgrid, nanogrid and peer-to-peer energy trading, power distribution faults, power system protection, signal detection

1 | INTRODUCTION

Renewable energy sources (also referred to as Distributed Renewable Energy (DER) or Distributed Generating (DG)), such as solar and wind are connected to the grid and microgrid (MG) seamlessly to supply power securely and reliably [1]. The use of DG offers several advantages, including lower carbon emissions, reduced transmission and distribution line upgrades, improved voltage profiles, lower losses, greater efficiency, and increased system stability, leading to cost savings. On the other hand, different forms of scattered resources, controlled load,

and generalised load can be blended to reduce dependency on the main grid [2]. Although distributed generation provides many advantages, there are some drawbacks as well. DG coupled directly to the main grid has a considerable negative impact as intermittent distributed resources are weather-dependent, volatile, and inconsistent, meaning that its power supply is not constant to maintain voltage and frequency.

In a DG-integrated microgrid, DGs can supply power to the microgrid until the grid supply becomes available. Without the primary grid supply, intermittent DGs cannot ensure the safety and quality of the power supply, which would necessitate

This is an open access article under the terms of the [Creative Commons Attribution](https://creativecommons.org/licenses/by/4.0/) License, which permits use, distribution and reproduction in any medium, provided the original work is properly cited.

© 2024 The Author(s). *IET Smart Grid* published by John Wiley & Sons Ltd on behalf of The Institution of Engineering and Technology.

the implementation of necessary safety procedures [3]. Islanding is the scenario that occurs when the load receives consistent energy from the DG during a main grid outage. An instance of islanding is represented by a distribution feeder connected to a DG-integrated microgrid as depicted in Figure 1. The figure illustrates a microgrid-based islanding system, where in the event of a failure that causes the circuit breaker to trip, the local load that remains may be supplied by the DG. During islanding, the voltage and frequency in the isolated region cannot be regulated by the primary grid. When islanding happens in power systems, workers in the field, system equipment, line recovery, and circuit breaker reclosing procedures are all in danger. Because of this, it is important to recognise islanding situations very quickly. When islanding happens, most utilities now need DG to be cut off from the network as soon as possible [4].

1.1 | Literature review

There are two distinct kinds of islanding: deliberate islanding and accidental islanding. Intentional islanding happens when the utility intentionally creates the island so that it can perform maintenance work. The unintentional islanding occurs when small power plants are cut off from the main electrical network for a variety of reasons, including bursting lines, defective equipment, operational error, natural hazards etc., [5]. The unintentional islanding creates problems, such as bi-directional energy flow that may place utility workers' lives at risk. Harmonic distortion, voltage regulation, and the stability of the power system are all issues to worry about with reverse power flow. Deviations from the set level of voltage and frequency can cause appliances to malfunction.

One of the major challenges in islanding detection is the detection of islanding quickly and precisely. Islanding detection is important because it prevents equipment damage, improves personal safety, and keeps utility operations running. Some standards and utility codes require protection against the islanding condition. In addition to offering security, privacy, and dependability, these codes are responsible for implementing these standards in practice. These standards were developed by organisations, such as IEEE and IEC and are regularly updated to account for the growing significance of

islanding detection in DG-linked grids [6]. An islanded DG should be detached from the mains within 2 s, as per the usual recommendations for islands with DG [7].

The various techniques for islanding detection are addressed in different research studies. Local and remote islanding detection methods (IDM) are divisions of IDM. Local approaches are built on measurements of specific features or factors on the grid side. These local methods have been further divided into active and passive methods. Active approaches typically operate on the premise that an external signal is fed into the network and that the DG outcomes are significantly affected by the appearance of an islanding state. When operating in a grid-connected state, the inserted signal is not considerably affected, but the system does exhibit an effective fluctuation when an islanding situation arises [8]. Numerous active approaches, such as Active Frequency Distortion (AFD) and Sandia Voltage Shifting (SVS) are analysed in the literature sources cited in refs. [9, 10]. Techniques such as Sandia Frequency Shifting (SFS) [11, 12] and Slip Mode Frequency Shifting (SMS), which entail alterations to the phase of current, are explored in refs. [13, 14]. The literature sources cited in refs. [15, 16] describe active approaches based on frequency jump and impedance measurement (IM). Active techniques are noted for their capability to detect islanding even when the supply and load are perfectly balanced, which leads to the creation of a Non-Detection Zone (NDZ). However, these active methods' main drawback is that, if the system is handled improperly, they may have a detrimental effect on the quality of the power.

In passive techniques, Point of Common Coupling (PCC) is employed for frequency monitoring, voltage, or power at the PCC location. To identify instances of islanding, fluctuations in these factors are tracked. There have been multiple applications for passive islanding techniques for identification in the past, including Under/Over Frequency Prevention (U/OFP), Rate of Change of Output Power (ROCOP), Rate of Change of Frequency (ROCOF), Total Harmonic Distortion (THD), phase Jump Detection (PJD), and Under/Over Voltage Prevention (U/OVP) [17]. The authors in ref. [18] propose a passive islanding method based on (O/UFP) and (O/UVP) to recognise the islanding condition. Voltage and current are determined at the PCC in an integrated power system. Voltage and frequency deviations from average values occur during islanding. If the measured value crosses the predefined value, an islanding scenario is detected. The voltage and current at DG connections are monitored for an abrupt phase jump using the PJD approach [19].

During islanding, per-phase angle variation is measured against the current threshold value. In ref. [20], the authors suggest an IDM for identifying islanding incidents based on the ROCOF. In an actual scenario, the suggested IDM keeps an eye on the current and frequency all the time to identify islanding as it happens. To distinguish between an islanding scenario and one where there are no islands, threshold values are used. The objective of the authors in ref. [21] was to identify trustworthy passive applicants for anti-islanding protection. ROCOP is used to track the output power (active and

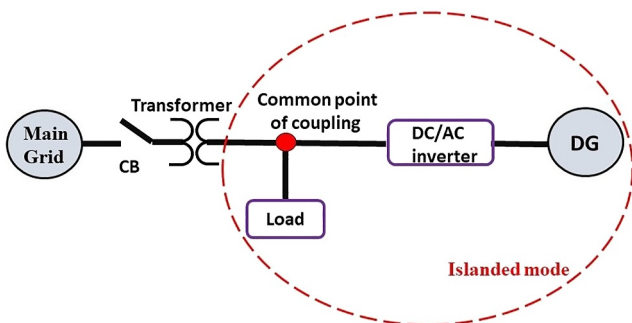


FIGURE 1 Microgrid-based islanding system.

reactive) at the PCC. The approach takes islanding into account if the variation rate goes above a certain point. Voltage unbalance occurs in the islanding mode in ref. [22] as a result of modifications to the network's architecture and load. Therefore, if the inconsistency in the 3-phase DG operating voltage is constantly checked, islanding can be effectively identified [23]. Preference is given to passive technologies due to their lower installation requirements and cost. The protective system can be implemented without extensive modifications, as it is budget-friendly. Since passive methods do not need to adjust to perturbations, they are faster than active techniques.

The primary issue with passive strategies is that they have a very large NDZ. This is because if the gap between load and supply is negligible, they may be unable to identify an island. For passive approaches to effectively detect islanding, careful consideration must also be given to setting appropriate threshold values [24]. A lower threshold value could result in unwanted tripping, while higher values could prevent the identification of islanding conditions. Consequently, the identification is more prone to errors. To get over these problems, signal processing-based [25] and intelligent solutions can be applied. For rapid, accurate, and reliable detection, they are adjusted by employing intelligent methodologies and modern signal-processing technologies [26]. Common examples of intelligent and signal processing-based classifier techniques include the Wavelet Transform (WT), Time-Time Transform (TTT) [27], Hilbert Huang Transform (HHT), Fourier Transform (FT), Support Vector Machine (SVM) [28], Artificial Neural Network (ANN) [29], S-Transform (ST) [30], Fuzzy Logic (FL) [31] and Decision Tree (DT) [32]. The signal processing-based IDMs can identify the islanding condition and other power quality concerns more precisely by leveraging the extremely distinctive features generated by WT, FT, HHT, ST, and TTT [33]. They work much better than traditional systems in terms of accuracy and speed of detection without lowering the quality of the power.

The remote technique depends on DG and utility communication. The primary benefits of remote methods include a minimal NDZ, a high level of reliability, better performance, and no impact on the quality of power [34]. There are several disadvantages of the remote technique which include higher expense, operational complexity, processing burden on the system, and disturbance in the operation due to failure in the communication link. Transfer trip schemes [35], Power Line Carrier Communication (PLCC) [36], and Supervisory Control and Data Acquisition (SCADA) [37] are all the most common examples of remote techniques.

1.2 | Contributions

In this research work, we integrate both inverter-based and synchronous DGs, utilising an innovative passive islanding identification technique. The technique starts with computing a 3-phase current signal at the PCC, followed by determining the Modal Current Envelope (MCE) using a range of demodulation methods, including the synchronous real demodulation

method, the asynchronous square law demodulation method, the complex square law demodulation method, and the quadrature demodulation method. Then, the autocorrelation function (ACF) is extracted through the envelope signal to eliminate further harmonics and obtain a significant number of samples. The generated sample deviation is then utilised as a metric for islanding detection. This proposed method is simple, fast, and exhibits a low neutral-to-ground voltage. The primary contributions of this paper are outlined below:

- The passive approach is proposed, which is based on a variation in the ACF of the MCE technique.
- The suggested technique uses only the current signal to recognise the islanding state.
- The method identifies the islanding circumstances with a smaller NDZ.
- Utilising the suggested technique, the detection time is greatly improved.
- Standard tests are used to thoroughly assess the system from all perspectives. It is also compared to other similar systems in terms of performance.

The remainder of the document is arranged as follows: Section 2 gives a detailed explanation of the recommended methodology. In Section 3, simulations and case studies are used to show how effective the recommended approach is. Finally, a conclusion and discussion are discussed in Sections 4 and 5.

2 | IMPLEMENTED ISLANDING DETECTION TECHNIQUES

The paper employs a passive islanding detection method using the changes in the Variance Autocorrelation Function of the Modal Current Envelope (VAMCE) for synchronous and inverter types of DGs. In this approach, the variance in the Autocorrelation Function (ACF) is used to detect the envelope. The methodology begins with the computation of the 3-phase current signal at the PCC, followed by the determination of the MC envelope using various demodulation methods.

2.1 | Modal current (MC)

A set of multiple data choices that show a certain level of mutual reliance because they all reflect the same material reality is known as a modal signal. When attempting to detect the condition of the islanding in the electric power network, it is important to recognise that every 3-phase current consists of a sequence of unbalanced data points. Transforming these currents into an MC signal leads to a substantial reduction in the amount of computation time and memory usage required. To extract the MC indication from a whole data set, the phase currents are mixed linearly [38].

$$I = \alpha I_a + \beta I_b + \gamma I_c \quad (1)$$

Here, I signifies a 3-phase modal current signal. The variables I_a , I_b , and I_c represent per-phase current measurements. In the above expression α , β , and γ stand for modal variables. α , β , and γ the modal variables would be chosen as 1, 2, and -3 , respectively. To prevent addition and subtraction between any two stages, each phase signal is scaled with a different variable. For every two-phase signal mix, this phase ensures that transient information is not neutralised [39]. Using this method, developing states can maintain all necessary transitory data in the reproduced signals.

The threshold value for the ACF (Autocorrelation Function) of the modal current (MC) envelope signal is determined based on the statistical properties of the signal variance. Specifically, in the balanced condition, the 3-phase current signal from IIDG-5 (inverter interface DG) is first transformed into an MC signal. The envelope of this MC signal is then extracted through quadrature demodulation. The ACF of this envelope signal is calculated, and its variance is analysed to set a threshold limit. This threshold is selected to distinguish normal operating conditions from potential anomalies.

2.2 | Schematics and working principles of envelope detection techniques

The envelope device combines all the maxima of the received data that is, a signal envelope is the same as its contour. Because it does not make use of frequency or the carrier signal, the envelop detector is a non-coherent device. The following techniques are employed in this paper to detect the message signal envelope:

- Synchronous real envelope detection
- Asynchronous complex square law envelope detection
- Square law envelope detection
- Quadrature envelope detection

When using a synchronous actual envelope recognition method, the native carrier signal multiplies the input signal before sending the output to a low-pass filter (LPF). In the asynchronous complex square law demodulation method, the Hilbert transform is used to create the analytical signal of the input in this envelope detection technique. In an analytical signal, the Hilbert transformation is the fictitious element, whereas the original output is the actual part. Hilbert's transformed value is squared and then square-rooted before sending it to the LPF. With square law demodulation, the input signal is simply multiplied by itself before being sent to the LPF. The quadrature demodulation technique can extract information from waveforms that are modulated in amplitude, frequency, or phase. The quadrature demodulation strategy employs two locally generated carrier signals that are phase-shifted by 90° from one another.

Then, the LPF receives the input signals and produces two squared components. The envelope signal is retrieved by adding these components and then computing the square root of the sum. To further separate the distorted components, a

large number of samples were generated by deriving ACF from the envelope signal. Therefore, island recognition is based on a measure of the generated samples' variability. Hence, the offered technique is a cost-effective option.

The method was tested using a modified version of the IEEE-399 standardised testing methodology [6]. Detecting islanding relies partially on signatures in the MC envelope. All of the 3-phase current transient properties are present in the MC envelope signal, so it is better to use the MC envelope signal to find islanding instead of just passive methods. Using the VAMCE method, under normal operating conditions, the criterion does not change much, but there is a big difference in the islanding operating mode.

Figure 2 illustrates the processed diagram for the proposed VAMCE technique with a synchronous real envelope detection method. MC output was created from the predicted 3-phase current signal. Actual envelope recognition is used to compute the signal's envelope, and ACF with acceptable latency is used to select the significant samples from the envelope signal. At this point, the variability of these specimens is calculated, and VAMCE is applied as a detection measure. Figure 3 shows a block schematic of the suggested approach using an actual envelope identification technique.

Figure 4 displays the process chart for the suggested VAMCE technology using an asynchronous complex square law envelope detection method. An MC signal is created from the predicted 3-phase current signal from PCC. The envelope is then computed using the complicated square law envelope detecting method, and the significant samples are subsequently extracted from the envelope signal using ACF at an appropriate delay. At

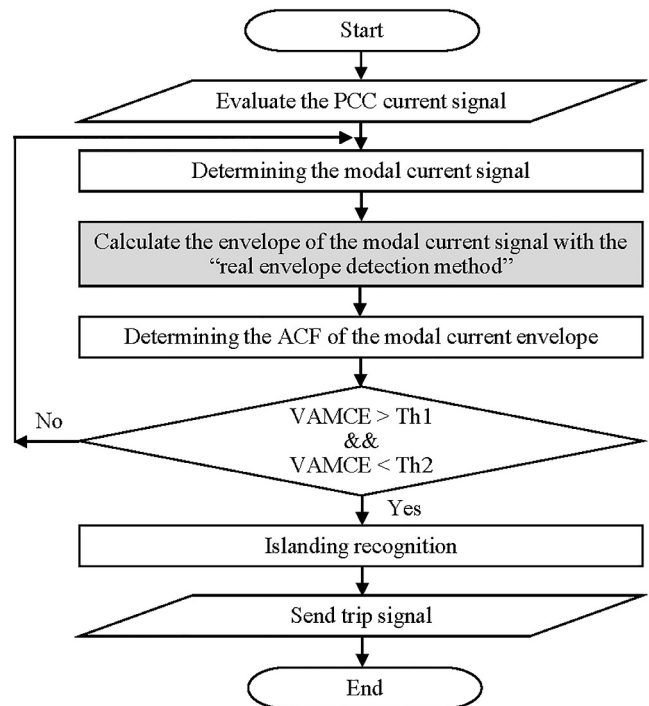


FIGURE 2 Flow chart of proposed VAMCE technique with synchronous real envelop detection.

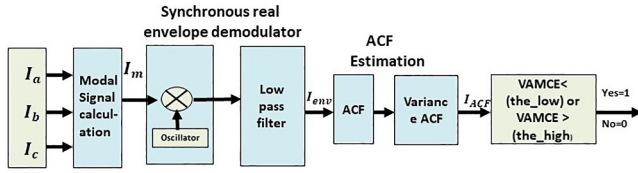


FIGURE 3 Block diagram of the proposed method with real envelope detection method.

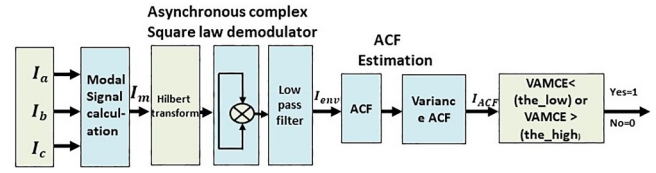


FIGURE 5 Block diagram of the proposed method with asynchronous complex square law envelope detection method.

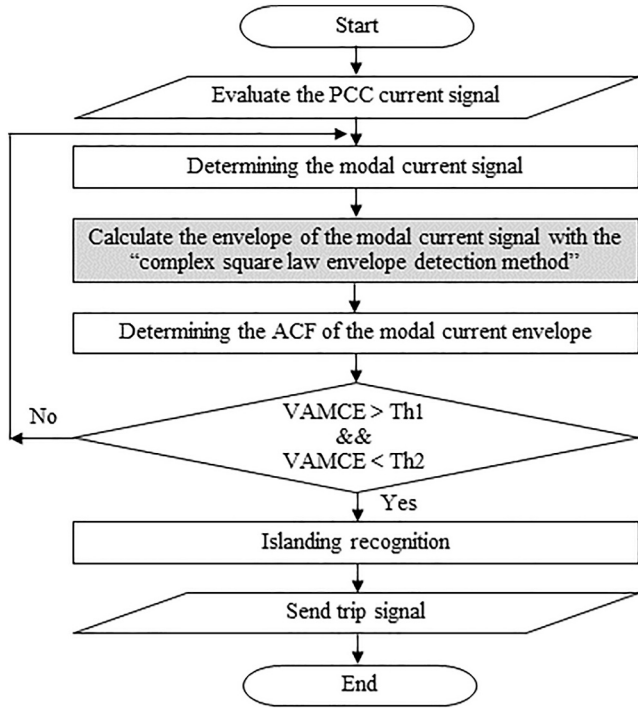


FIGURE 4 Flow chart of proposed VAMCE technique with asynchronous complex square law envelope detection.

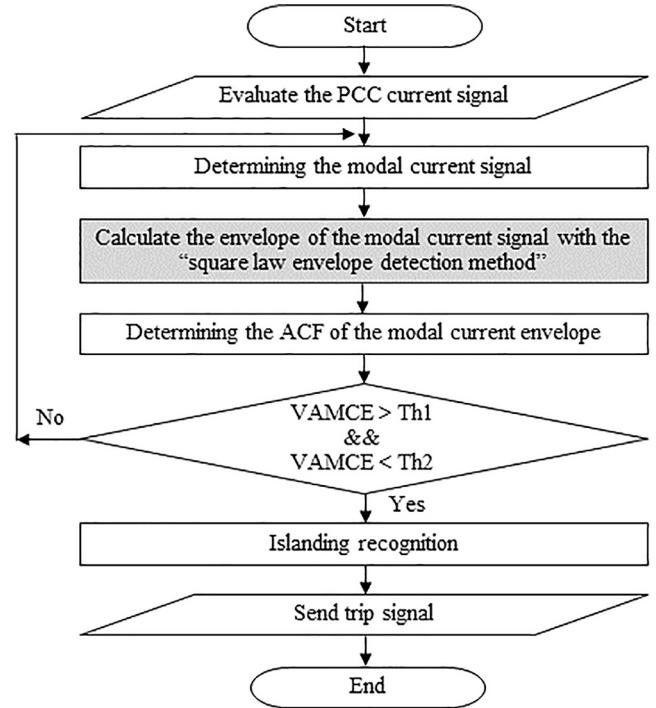


FIGURE 6 Flow chart of proposed VAMCE technique with square law.

this stage, the variability of these specimens is calculated, and VAMCE is applied as a detection measure. Figure 5 displays a block schematic of the suggested technique with an asynchronous complex square law envelope detection method.

Figure 6 illustrates a flow chart for the suggested VAMCE technique using the square law envelope detection method. The signal at PCC indicates that the anticipated 3-phase current is changed into an MC signal. The square-law envelope recognition technique is used in this procedure to compute the envelope. Now, the essential samples from the envelope signal are extracted with the assistance of ACF and a reasonable amount of delay. At this juncture, VAMCE serves as a detection measure once the variation of these samples is computed. Figure 7 demonstrates a block schematic of the suggested approach using the envelope detection technique of square law.

A flow chart for the proposed VAMCE technique with quadrature demodulation is shown in Figure 8. An MC output is created by PCC from the predicted 3-phase current signal. Currently, the envelope is calculated via quadrature envelope detection. To extract the relevant samples from the envelope signal, we first employ ACF with an appropriate latency. Here,

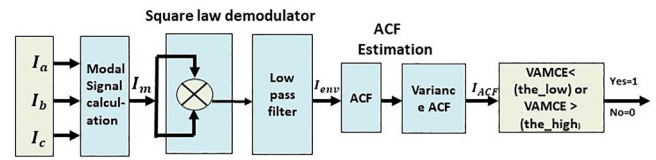


FIGURE 7 Block diagram of the proposed method with square law envelope detection method.

we calculate the sample variance and employ VAMCE as a detection method. Figure 9 shows a block schematic of the proposed method with quadrature demodulation. A trip signal is created if the criterion (VAMCE) exceeds the predefined threshold, which is interpreted as an islanding circumstance.

2.3 | Mathematical expressions of envelope detection techniques

Detailed equations of the four implemented techniques have been presented below.

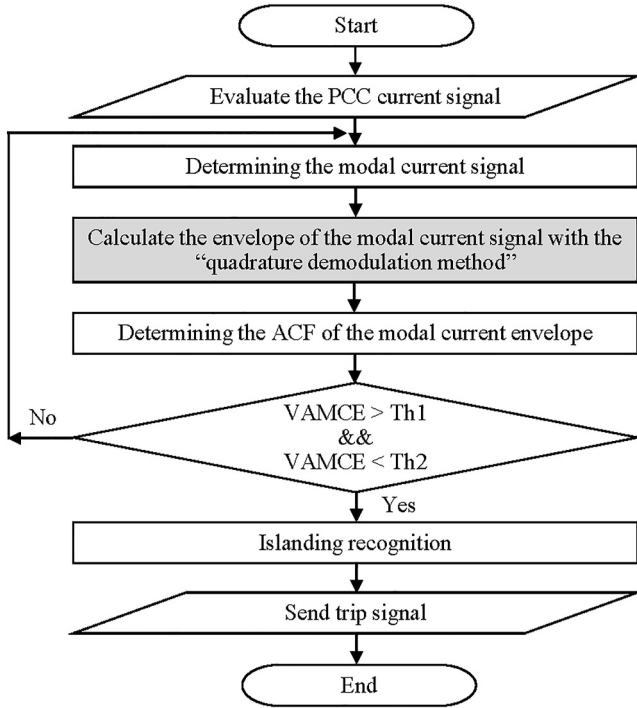


FIGURE 8 Flow chart of proposed VAMCE technique with quadrature envelope detection.

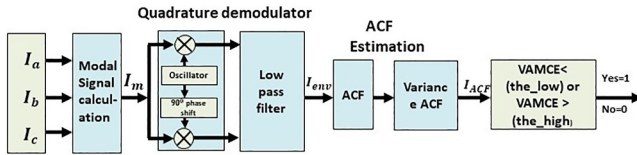


FIGURE 9 Representation of proposed method in block diagram with quadrature envelope detection method.

2.3.1 | Synchronous real envelope detection

In synchronous real envelope detection, the product is formed by multiplying the input signal with the local carrier signal. After multiplication, the output signal is sent to the LPF. The LPF is used in this method to remove the high-frequency information and to recover the envelope signal.

In synchronous real envelope detection, the two signals are used.

- Double sideband transmitter carrier (DSB TC) AM signal can be represented as follows,

$$DSB_{tc}(t) = [(y(t) + C_r) \cos(2\pi f_{cr}t)] \quad (2)$$

- Local carriers can be represented as follows,

$$C_{lc} = \cos(2\pi f_{cr}t) \quad (3)$$

where, C_r : Carrier amplitude, t : Time and f_{cr} : Carrier frequency. When these two signals are fed into the mixer, the output can be represented as follows:

$$\begin{aligned} & DSB_{tc}C_{lc} \\ &= [(y(t) + C_r) \cos(2\pi f_{cr}t) (\cos(2\pi f_{cr}t))] \\ &= [y(t) \cos(2\pi f_{cr}t) \cos(2\pi f_{cr}t)] \\ &\quad + [C_r \cos(2\pi f_{cr}t) \cos(2\pi f_{cr}t)] \quad (4) \\ &= y(t) \cos^2(2\pi f_{cr}t) + C_r \cos^2(2\pi f_{cr}t) \\ &= [y(t) + C_r] \cos^2(2\pi f_{cr}t) \end{aligned}$$

By using the formula $\frac{(1 + \cos(2\theta))}{2}$ Eq. (4) becomes:

$$\begin{aligned} &= [y(t) + C_r] \frac{1 + \cos(4\pi f_{cr}t)}{2} \\ &= \frac{1}{2}(y(t) + C_r) [\cos(4\pi f_{cr}t) + 1] \quad (5) \\ &= \frac{1}{2}(y(t) + C_r) + \frac{1}{2}(y(t) + C_r) \cos(4\pi f_{cr}t) \end{aligned}$$

In Eq. (8) $\frac{1}{2}(y(t) + C_r) \cos(4\pi f_{cr}t)$ is the high-energy part; hence, the original message signal remains after the high-frequency portion is removed by passing through the LPF.

$$Y(t) = \frac{1}{2}(y(t) + C_r) \quad (6)$$

This $\frac{1}{2}(y(t) + C_r)$ is the demodulated signal.

The phase angle should be considered if there is any angle between the original signal and the local carrier. It is assumed that the phase difference is ϕ and the local carrier becomes $\cos(2\pi f_{cr}t) + \phi$. When DSB_{tc} signal is multiplied with $\cos(2\pi f_{cr}t) + \phi$, the output can be represented as follows:

$$\begin{aligned} &= [(y(t) + C_r) \cos(2\pi f_{cr}t)] \cos(2\pi f_{cr}t) + \phi \\ &= (y(t) + C_r) [(\cos(2\pi f_{cr}t)) (\cos(2\pi f_{cr}t) + \phi)] \quad (7) \end{aligned}$$

From the trigonometric function formula that is, $\cos \alpha \cos \beta = 1/2[\cos(\alpha + \beta) + \cos(\alpha - \beta)]$, by using this transformation Eq. (7) becomes,

$$\begin{aligned} &= (y(t) + C_r) \frac{1}{2} [\cos(2\pi f_{cr}t + 2\pi f_{cr}t + \phi) \\ &\quad + \cos(2\pi f_{cr}t - 2\pi f_{cr}t - \phi)] \\ &= (y(t) + C_r) \frac{1}{2} [\cos(4\pi f_{cr}t + \phi) + \cos(\phi)] \end{aligned}$$

$$= \frac{1}{2}(y(t) + C_r) \cos(4\pi f_{cr}t + \phi) + \frac{1}{2}(y(t) + C_r) \cos(\phi) \quad (8)$$

In Eq. (8), $\frac{1}{2}(y(t) + C_r) \cos(4\pi f_{cr}t + \phi)$ is the high-frequency part, which is eliminated from LPF and low-frequency component is left that is, $\frac{1}{2}(y(t) + C_r) \cos(\phi)$

$$Y(t) = \frac{1}{2}(y(t) + C_r) \cos(\phi) \quad (9)$$

This is the demodulated signal which is scaled by $\cos(\phi)$. So phase difference is not eliminated in this case.

2.3.2 | Asynchronous complex square law envelope detection

This envelope detection method first creates the input's analytical signal using the Hilbert transform. An analytical signal's original signal is its genuine component; the Hilbert transform of the actual signal is its imaginary portion. The Hilbert transform, which would be performed by an FIR filter, will add a delay of half the filter size; hence, it is essential to delay the input signal. After this, the output of the Hilbert transform generates two components that are squared with themselves, and in addition, to counter the effects of squaring the signal, which leads to distortion, the output signal is square-rooted and then processed by an LPF to eliminate any high-frequency components. Finally, the envelope signal is recovered.

The output of the DSB TC signal after passing through the Hilbert transform can be indicated as follows:

$$h_+(t) = h(t) + j\hat{h}(t) \quad (10)$$

where, $h_+(t)$ is the pre envelope signal, $h(t) = y(t) \cos(2\pi f_{cr}t)$ is the DSB TC signal and the Hilbert transform of $h(t)$ is $\hat{h}(t) = y(t) \sin(2\pi f_{cr}t)$.

After squaring of $(h_+(t))^2$ is defined as follows:

$$(h_+(t))^2 = (y(t) + Ac)^2 \cos^2(2\pi f_{cr}t) + (y(t) + Ac)^2 \sin^2(2\pi f_{cr}t) \quad (11)$$

Then take the square root of Eq. (11). The output is defined as follows:

$$= \sqrt{y(t) + Ac)^2 \cos^2(2\pi f_{cr}t) + (y(t) + Ac)^2 \sin^2(2\pi f_{cr}t)} \\ = \sqrt{(y(t) + C_r)^2 [\cos^2(2\pi f_{cr}t) + \sin^2(2\pi f_{cr}t)]} \quad (12)$$

From the trigonometric function formula that is, $\cos^2 \alpha + \sin^2 \beta = 1$, by using this transformation Eq. (12) becomes,

$$= \sqrt{(y(t) + C_r)^2} \\ h_+(t) = (y(t) + C_r) \quad (13)$$

Eq. (13) represents the demodulated signal.

2.3.3 | Square law envelope detection

The signal that is input is squared with itself in the square law method before the output is transmitted to the LPF. After that, an LPF filter is used to eliminate the high-energy signal. Finally, all that is left is the signal envelope.

In AM communication, a frequency carrier $C_r \cos 2\pi f_{cr}t$ of amplitude A is broadcast in addition to the modulated signal $y(t) \cos 2\pi f_{cr}t$, eliminating the requirement for the receiver to produce the carrier. As a result, the receiver is easier to use and less expensive. DSB TC signals are used in this system.

- Double sideband transmitter carrier (DSB TC) AM signal

$$DSB_{tc}(t) = (y(t) + C_r) \cos(2\pi f_{cr}t) \quad (14)$$

The output of the square law module is defined as follows:

$$= [(y(t) + C_r) \cos(2\pi f_{cr}t)]^2 \\ = (y(t) + C_r)^2 \cos^2(2\pi f_{cr}t) \quad (15)$$

By using the formula $\frac{(1 + \cos(2\theta))}{2}$ Eq. (15) becomes:

$$= \frac{1}{2}(y(t) + C_r)^2 [\cos(4\pi f_{cr}t) + 1] \\ = \frac{1}{2}(y(t) + C_r)^2 + \frac{1}{2}(y(t) + C_r)^2 \cos(4\pi f_{cr}t) \quad (16)$$

In Eq. (16) $\frac{1}{2}(y(t) + C_r)^2 \cos(4\pi f_{cr}t)$ is the high-frequency part, which a low pass filter can be used to remove and just the low-frequency part $\frac{1}{2}(y(t) + C_r)^2$ is left. The low-frequency component's square root is as follows:

$$= \sqrt{\frac{1}{2}(y(t) + C_r)^2} \quad (17)$$

$$Y(T) = \frac{1}{\sqrt{2}}(y(t) + C_r)^2 \forall t$$

The $Y(T)$ in Eq. (17) represents the signal which is demodulated and is identical to the initial information signal.

2.3.4 | Quadrature envelope detection

In quadrature demodulation, two local oscillator-generated carrier signals are used. Both carrier signals are multiplied by the input, one in the lower channel and the other with a 90° phase shift in the upper channel. Low-pass filters are necessary due to the similarity of the quadrature multiplier used in the receiver to a typical AM demodulator, which leads to a carrier frequency shift. The high-frequency components are removed by transmitting the signals to an LPF. The input, after being filtered, is separated into two parts: the in-phase part ($p(t)$) and the quadrature part ($T(t)$), which retain the original amplitude and phase information of the input. The two signals are amplified by a factor of 10 to retain half of the initial energy. The output is then square-rooted to eliminate any distortion and retrieve the envelope signal.

In amplitude modulation (AM) transmission, the original signal is altered and transmitted together with amplitude A and a high-frequency carrier signal. This process utilises two signals.

- Local carrier C_{lc} can be represented as follows:

$$\cos(2\pi f_{cr}t) \quad (18)$$

and

$$\sin(2\pi f_{cr}t) \quad (19)$$

- Double sideband transmitter carrier (DSB TC) AM signal can be represented as follows:

$$DSB_{tc}(t) = (y(t) + C_r) \cos(2\pi f_{cr}t) \quad (20)$$

where, C_r : Carrier amplitude, t : Time and f_{cr} : Carrier frequency.

In DSB-TC amplitude modulation, the $\sin(2\pi f_{cr}t)$ and $\cos(2\pi f_{cr}t)$ are multiplied with the input signal. Considering the phase difference, the local carriers are transformed to $\sin(2\pi f_{cr}t + \phi)$ and $\cos(2\pi f_{cr}t + \phi)$. After the multiplication of $\cos(2\pi f_{cr}t + \phi)$ with the DSB-TC, the output of the upper mixer will be represented as follows:

$$\begin{aligned} & DSB_{tc} \cdot \cos(2\pi f_{cr}t + \phi) \\ &= [(y(t) + C_r) \cos(2\pi f_{cr}t)] \cos(2\pi f_{cr}t + \phi) \quad (21) \\ &= (y(t) + C_r) [\cos(2\pi f_{cr}t) \cos(2\pi f_{cr}t + \phi)] \end{aligned}$$

From the trigonometric function formula that is, $\cos \alpha \cos \beta = 1/2[\cos(\alpha + \beta) + \cos(\alpha - \beta)]$, by using this transformation Eq. (7) becomes,

$$\begin{aligned} &= (y(t) + C_r) \frac{1}{2} [(\cos(2\pi f_{cr}t + (2\pi f_{cr}t + \phi))) \\ &+ (\cos(2\pi f_{cr}t - (2\pi f_{cr}t - \phi)))] \quad (22) \end{aligned}$$

After solving Eq. (4)

$$\begin{aligned} &= (y(t) + C_r) \frac{1}{2} [\cos(4\pi f_{cr}t + \phi) + \cos(\phi)] \\ &= \frac{1}{2}(y(t) + C_r) \cos(4\pi f_{cr}t + \phi) + \frac{1}{2}(y(t) \\ &+ C_r) \cos(\phi) \quad (23) \end{aligned}$$

The output of the lower mixer, when AM signal DSB_{tc} multiplied with $\sin(2\pi f_{cr}t + \phi)$, is given as follows:

$$\begin{aligned} & DSB_{tc} \cdot \sin(2\pi f_{cr}t + \phi) \\ &= [(y(t) + C_r) \cos(2\pi f_{cr}t)] \sin(2\pi f_{cr}t + \phi) \quad (24) \\ &= (y(t) + C_r) [\cos(2\pi f_{cr}t) \sin(2\pi f_{cr}t + \phi)] \end{aligned}$$

From the trigonometric function formula that is, $\cos \alpha \sin \beta = 1/2[\sin(\alpha + \beta) - \sin(\alpha - \beta)]$, by using this transformation Eq. (24) becomes,

$$\begin{aligned} &= (y(t) + C_r) \frac{1}{2} [\sin(2\pi f_{cr}t + \phi + 2\pi f_{cr}t) \\ &+ \sin(2\pi f_{cr}t - \phi - 2\pi f_{cr}t)] \quad (25) \end{aligned}$$

After solving Eq. (25)

$$\begin{aligned} &= (y(t) + C_r) \frac{1}{2} [\sin(4\pi f_{cr}t + \phi) + \sin(\phi)] \\ &= \frac{1}{2}(y(t) + C_r) \sin(4\pi f_{cr}t + \phi) + \frac{1}{2}(y(t) \\ &+ C_r) \sin(\phi) \quad (26) \end{aligned}$$

The high-frequency parts present in Eqs. (23) and (26) are removed by passing the signal through an LPF, which results in obtaining the in-phase component $S(t)$ and quadrature component $R(t)$. The high frequency component is represented by the expression $\frac{1}{2}(y(t) + C_r) \cos(4\pi f_{cr}t + \phi)$ and $\frac{1}{2}(y(t) + C_r) \sin(4\pi f_{cr}t + \phi)$.

$$P(t) = \frac{1}{2}(y(t) + C_r) \cos(\phi) \quad (27)$$

$$T(t) = \frac{1}{2}(y(t) + C_r) \sin(\phi) \quad (28)$$

By finding the magnitude of the in-phase current $S(t)$ and quadrature component $R(t)$, the original signal can be recovered.

$$[P^2(t) + T^2(t)]^{\frac{1}{2}} \quad (29)$$

By putting the values of $P(t)$ and $T(t)$, Eq. (29) becomes,

$$= \left[\frac{1}{4}(y(t) + C_r)^2 \cos^2(\phi) + \frac{1}{4}(y(t) + C_r)^2 \sin^2(\phi) \right]^{\frac{1}{2}} \quad (30)$$

$$= \sqrt{\left[\frac{1}{4}(y(t) + C_r)^2 (\cos^2(\phi) + \sin^2(\phi)) \right]}$$

From the trigonometric function formula that is, $\cos^2 \alpha + \sin^2 \beta = 1$, by using this transformation Eq. (30) becomes,

$$= \sqrt{\left[\frac{1}{4}(y(t) + C_r)^2 \cdot 1 \right]} \quad (31)$$

$$Y(T) = \frac{1}{2}(y(t) + C_r)$$

Once the phase difference (ϕ) is subtracted out, the demodulated output is the message signal $y(t)$ itself.

2.4 | Autocorrelation function

For islanding identification, the ACF of the envelope's result is the suggested criterion. Autocorrelation is a numerical method of obtaining signal data as a delayed variation. In simple terms, autocorrelation looks for a pulse that is similar to itself after a certain amount of time has passed. When discussing relatively short sequences, autocorrelation is frequently demonstrated in terms of constrained limitations over summing. For K samples, the following is the correlation among various model parameters, divided by their delays. The output sample variation will be used as an islanding recognition criterion.

$$G_l = \frac{\sum_{j=1}^{K-l} (x_j - \bar{x})(x_{j+l} - \bar{x})}{\sum_{j=1}^K (x_j - \bar{x})^2} \quad (32)$$

$$\bar{x} = \frac{\sum_{j=1}^K (x_j)}{K} \quad (33)$$

The signal value at the j th sample is represented by x_j . Average is represented by \bar{x} . The autocorrelation of output at delay l for the time series data x_j is called G_l , and it generally lies between -1 and $+1$.

3 | SIMULATION RESULTS

The proposed model is validated by a series of simulations to prove its worth. Many scenarios of balanced and unbalanced loads are simulated to test the islanding functionality. The IEEE 929–1988 standard states that the MG must be disconnected as soon as a network is islanded [40]. The IEEE

1547–2003 [41, 42], IEEE 929–2000, and IEC-62116 standards provide a maximum delay of 2 s in the event of low-level faults. However, the VAMCE decision criteria for islanding detection is the maximum delay of 2 s. The proposed method was applied to the IEEE 399 distribution network, with modifications made to accommodate the decentralised nature of microgrids (MGs) [6].

The test system, seen in Figure 10, is a one-line schematic of the system under study. To evaluate the effectiveness of the proposed method, MATLAB/Simulink simulations were performed. It was constructed with 5 MGs, and the main grid had a power component ratio of 7 X/R and a 500 MVA short-circuit limit. Both of the 25-high-voltage distributions in the test system were connected to the main grid via a 120/25 MVA (phase-to-phase) step-down converter. The ring distributors of the framework were wired to loads L1–L6. There were six RL branches carrying loads from L1 to L6, with L5 serving as a 3-phase source. There is one 3 MW inverter interface DG (IIDG-5) and one 4 MVA synchronous generator (SG-3) connected to the network via distributor F-2.

Test system parameters are shown in Table 1. A synchronous generator (SG-1) with a 4 MVA rating is linked to an inverter interface (IIDG-1) with a 3 MW rating on F-3. One 4-MVA synchronous generator (SG-2) is placed in F1's distributor. Each IIDG system has a built-in voltage regulator. Opening the switch near their respective producing units will allow SG-1 connected to the first bus and IIDG-5 connected

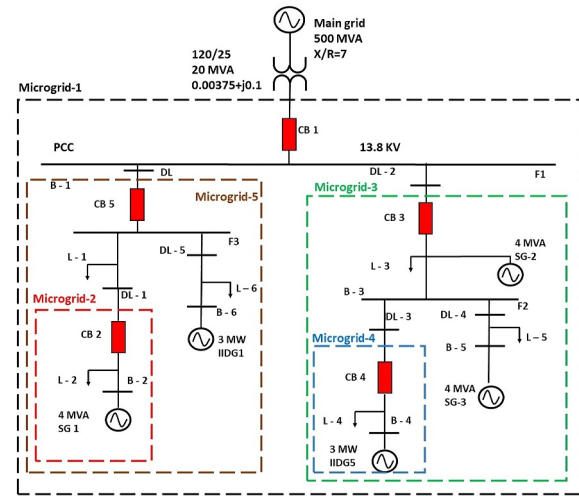


FIGURE 10 Representation of test system using single line diagram.

TABLE 1 Parameters of test system.

Quantity name	Value
Voltage rating	13.80 kV
IIDG-5 minimum power	4.0 MVA
IIDG-1 minimum power	3.0 MW
Sampling frequency	3600.0 Hz
Nominal DC bus voltage	500.0 V

to the fourth bus to experience several frequent islanding scenarios. Simulations were performed to examine the islanding scenarios, yet only a limited number of accurate results are displayed in the subsequent sections.

3.1 | Case 1: Synchronous real envelope detection

3.1.1 | Balanced condition for generation and load

For each island identification technique, it is found that the generating and distributing load phases have the least adverse consequences. The goal of this study is to demonstrate that, in certain circumstances, this approach is successful in locating islanding. A load L-2 as shown in Figure 10, of 4 MVA is imposed during testing to evaluate the balanced state in MG-2. In the suggested method, the 3-phase current signal from SG-1 shown in Figure 10 is used and transformed into an MC signal. Figures 11 and 12 show the simulated 3-phase current and MC signals, respectively. Subsequently, the MC signal envelope is established by simultaneous real demodulation. Limits are established when the ACF of the signal has been determined; this provides a variance sample. In this scenario, CB-2 in Figure 10 is unlocked, and the switching transition stage is 0.7 s long, with a delay of a few milliseconds to represent an islanding condition. The switching of circuit breakers depends upon the variance sample of ACF. In balanced conditions for

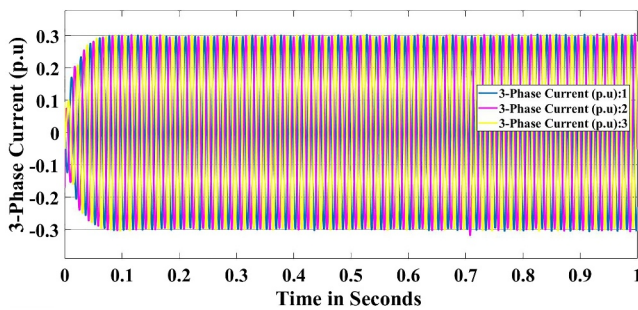


FIGURE 11 Case 1: Current signals in 3-phase generation and load balance condition.

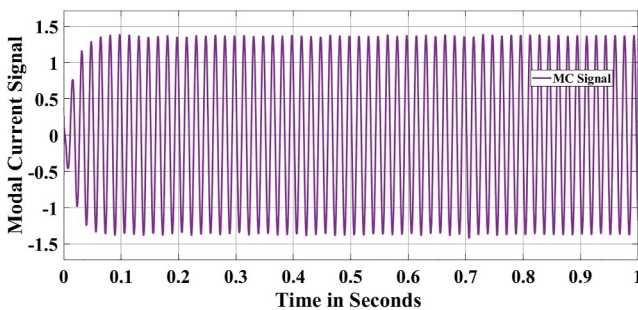


FIGURE 12 Case 1: MC signal in generation and load balanced condition.

generation and load, the output power remains the same after tripping. The VAMCE output with tripped in this islanding state is depicted in Figure 13.

3.1.2 | Unbalanced condition for generation and load

In this scenario, a load L-2 of approximately 4 MVA is applied to MG-2 to examine the generation and load imbalance. The 3-phase current signal from SG1 is utilised in the proposed method and converted into a modulated carrier signal. The simulated results of 3-phase current and MC signals in an imbalanced state are presented in Figures 14 and 15, respectively. The MC envelope of a signal is found using the Synchronous Actual Envelope Demodulation process.

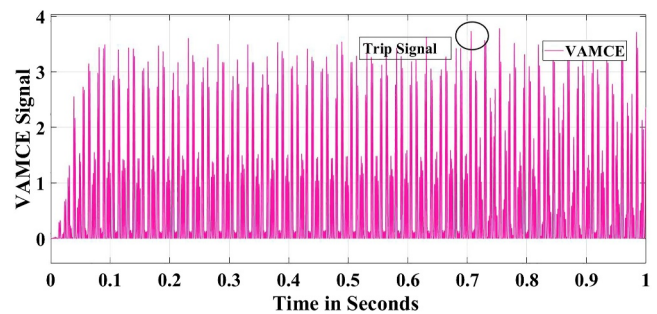


FIGURE 13 Case 1: VAMCE with trip signal in generation and load balanced condition.

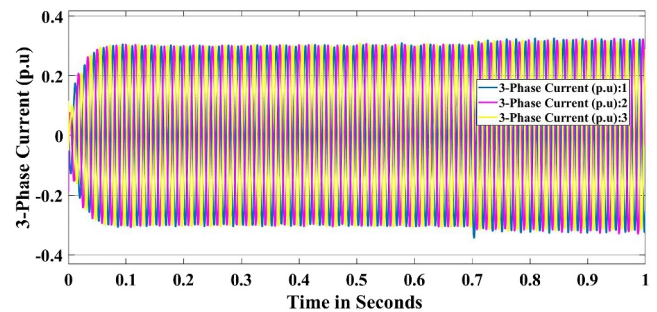


FIGURE 14 Case 1: 3-phase current signal in generation and load unbalanced condition.

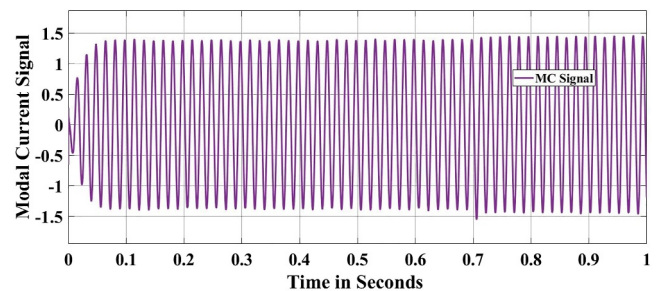


FIGURE 15 Case 1: MC signal in generation and load unbalanced condition.

Subsequently, Following the computation of the signal's ACF, a variance sampling and an acceptable threshold limitation are established. A scenario of islanding is simulated by opening CB-2 for 0.7 s with a delay of several milliseconds, and the resulting VAMCE signal with tripping is depicted in Figure 16. In unbalanced conditions for load and generation, the output power slightly changes after the tripping.

3.2 | Case 2: Asynchronous complex square law envelope detection

3.2.1 | Balanced condition for generation and load

The goal of this study is to show that the suggested method performs better in these situations to detect islanding. During the testing process, a load L-2 shown in Figure 10 of about 4 MVA is applied to observe the balanced condition in MG-2. In the proposed method, SG-1's 3-phase current signal is utilised and transformed into an MC signal. Simulation results of the 3-phase current signal and MC signal are seen in Figures 17 and 18, respectively. Then the MC envelope of the MC signal is found by asynchronous complex square law envelope detection. Then, After determining the signal's ACF, which produces an irregular sample, the threshold limitation is established. CB-2 in Figure 10 is open for simulating an islanding condition in this circumstance, with the switching transition stage of 0.6 s with a delay of about a few

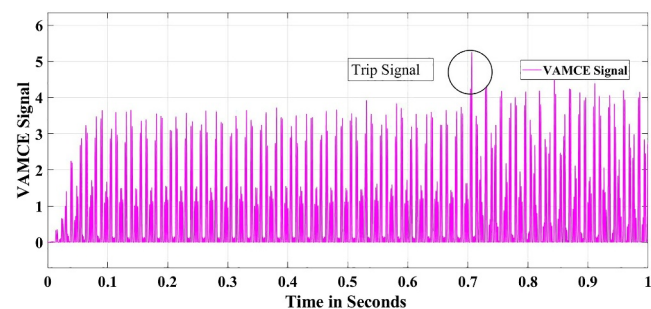


FIGURE 16 Case 1: VAMCE with trip signal in generation and load unbalanced condition.

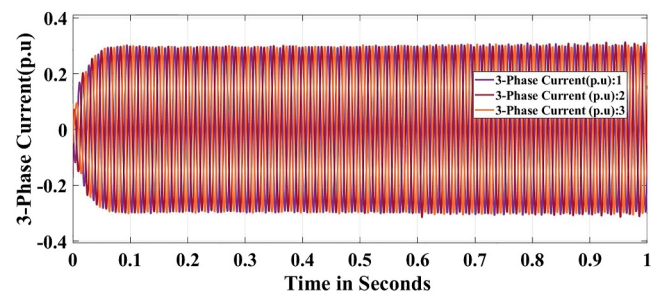


FIGURE 17 Case 2: 3-phase current signal in generation and load balanced condition.

milliseconds. Figure 19 shows the VAMCE signal with tripping during this islanding condition.

3.2.2 | Unbalanced condition for generation and load

In this scenario, a load L-2 of about 4 MVA (see Figure 10) is applied to observe the generation and load unbalanced conditions in MG-2. In the proposed method, SG-1's 3-phase current signal (see Figure 10) is utilised and transformed into an MC signal. Simulation results of the 3-phase current signal and the associated MC signal in an imbalanced state are displayed in Figures 20 and 21, respectively. The MC envelope of the MC signal is then calculated through asynchronous complex square law envelope detection. Next, the autocorrelation

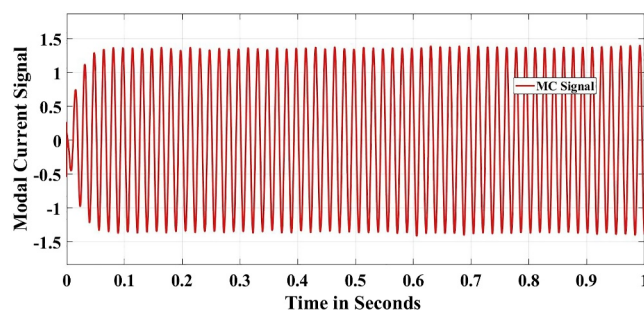


FIGURE 18 Case 2: MC signal in generation and load balanced condition.

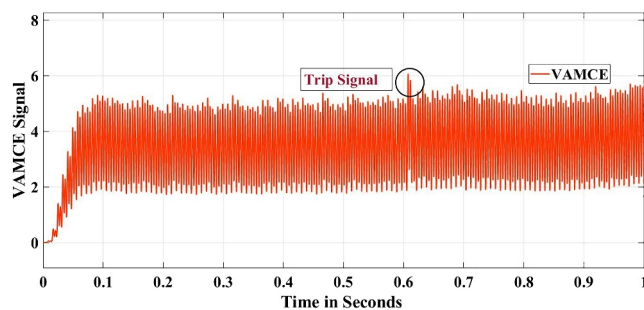


FIGURE 19 Case 2: VAMCE with trip signal in generation and load balanced condition.

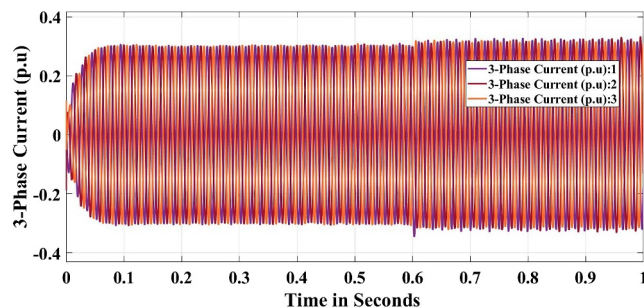


FIGURE 20 Case 2: 3-phase current signal in generation and load unbalanced condition.

of the signal is determined, providing a sample of the variance, and a threshold limit is established. CB-2 was enabled for 0.6 s adding a few milliseconds of delay to mimic islanding. Figure 22 displays the VAMCE signal while tripping in this state of islanding.

3.3 | Case 3: Square law envelope detection

3.3.1 | Balanced condition for generation and load

The IIDG5 MC signal and 3-phase current simulation resulting in a load-generation balanced condition for MG-4 are presented in Figures 23 and 24. To observe the balanced condition of MG-

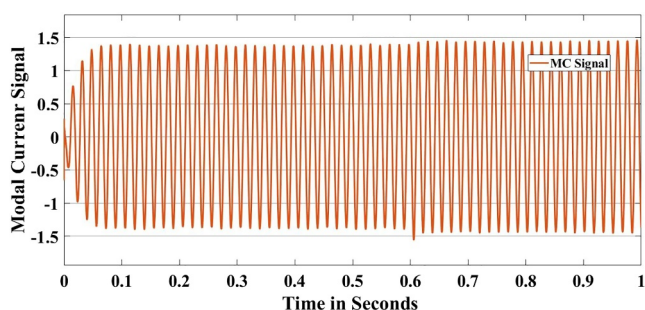


FIGURE 21 Case 2: MC signal in generation and load unbalanced condition.

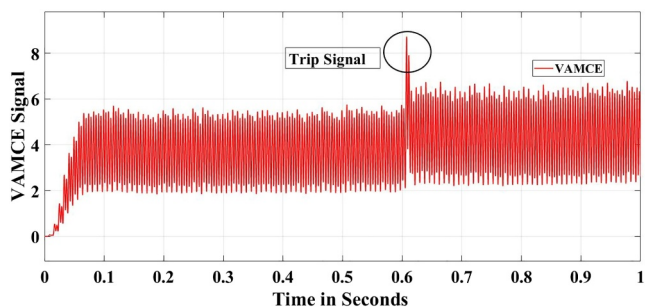


FIGURE 22 Case 2: VAMCE with trip signal in generation and load unbalanced condition.

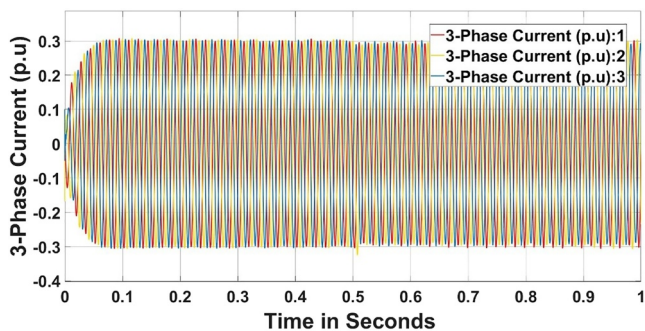


FIGURE 23 Case 3: 3-phase current signal in generation and load balanced condition.

4, a load of approximately 3 MW was applied to L-4 during the testing phase. Although there may be slight changes in the signal as a result of the balanced condition, an NDZ is anticipated for passive systems. The simulation for the VAMCE approach along with the islanding detection trip signal for IIDG5 is demonstrated in Figure 25. The CB-4 was opened with a switch transition period of 0.5 s to establish an islanding state.

3.3.2 | Unbalanced condition for generation and load

For the load-generation mismatch scenario, MG-4 was used. The linked load in MG-4 exceeds IIDG-5's capacity restrictions as shown in Figures 26 and 27. The current

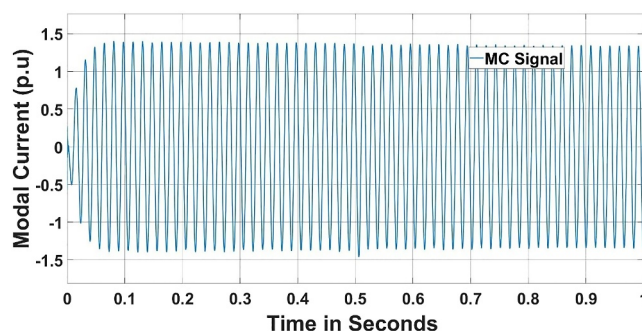


FIGURE 24 Case 3: MC signal in generation and load balanced condition.

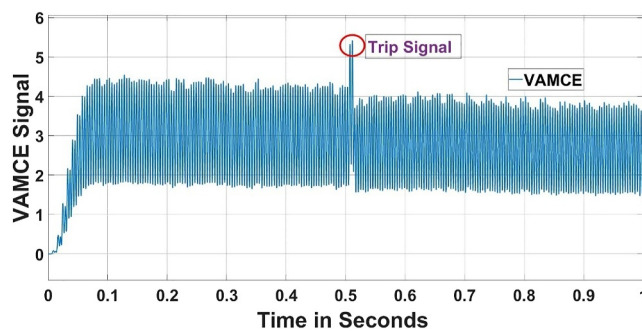


FIGURE 25 Case 3: VAMCE with trip signal in generation and load balanced condition.

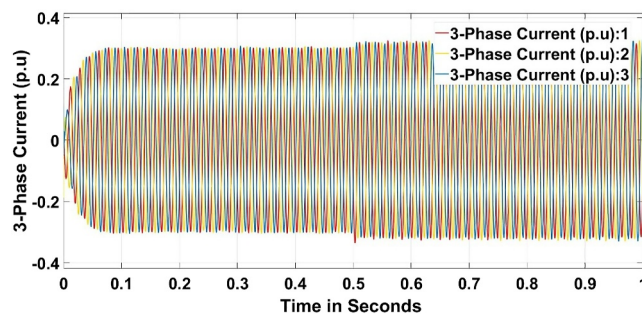


FIGURE 26 Case 3: 3-phase current signal in generation and load unbalanced condition.

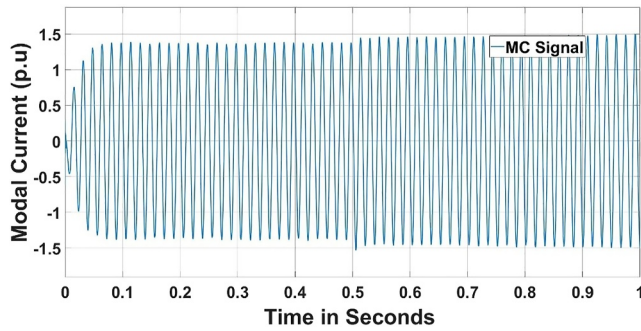


FIGURE 27 Case 3: MC signal in generation and load unbalanced condition.

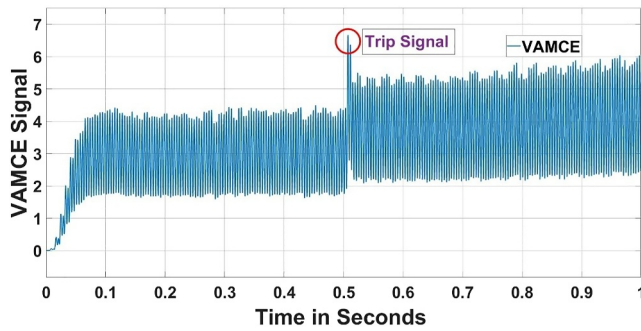


FIGURE 28 Case 3: VAMCE with trip signal in generation and load unbalanced condition.

indication on the DG terminal noticeably changes when islanding occurs because there is an abrupt change in the DG loads in MG-4. The VAMCE trip indication during the islanding incident is shown in Figure 28. To simulate islanding in this instance, the CB-4 was unlocked at 0.5 s.

3.4 | Case 4: Quadrature envelope detection

3.4.1 | Balanced condition for generation and load

MG-4 (as shown in Figure 10) is subjected to a load of roughly 3 MW during testing in order to evaluate the balanced state. The fluctuation in the current signal is minimal under balanced conditions, leading to the assumption of an NDZ in passive systems. However, the proposed method effectively addressed this issue. The 3-phase current signal from IIDG5 was transformed into an MC signal using the proposed approach. The simulated results of the 3-phase current signal and MC signal are depicted in Figures 29 and 30, respectively. The MC envelope of the MC signal is determined through quadrature demodulation, and the ACF has been calculated to determine the signal's variance and set the threshold limit. The switching transition stage is set to 0.4 s, with a few milliseconds of delay, enabling CB-4 to simulate an islanding condition. The results, as shown in Figure 31, demonstrate that the VAMCE signal exhibits a considerable range of variability during this islanding scenario.

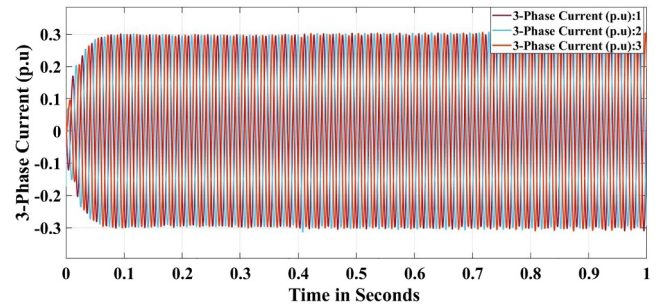


FIGURE 29 Case 4: 3-phase current signal in generation and load balanced condition.

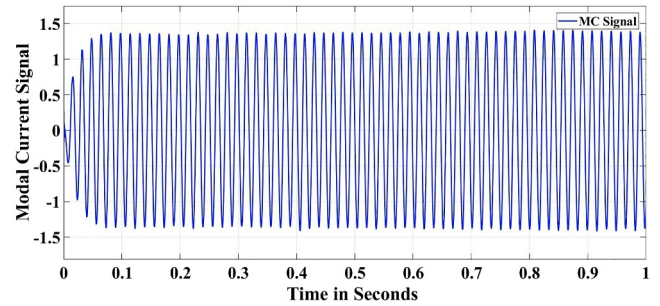


FIGURE 30 Case 4: MC signal in generation and load balanced condition.

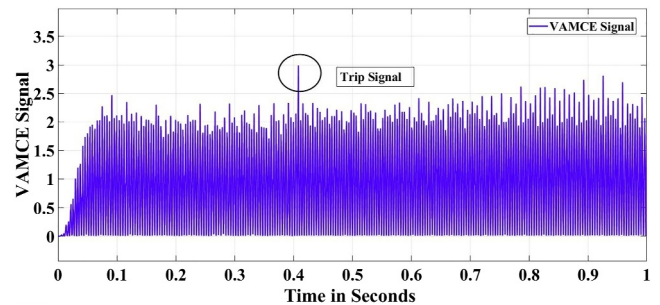


FIGURE 31 Case 4: VAMCE with trip signal in generation and load balanced condition.

3.4.2 | Unbalanced condition for generation and load

During the assessment of the unbalanced condition in MG-4, a load of approximately 3 MW (as depicted in Figure 10) is applied to L-4. The 3-phase current signal from IIDG5 is utilised in the proposed method and transformed into an MC signal. The 3-phase current signal and MC signal simulation outcomes in the imbalanced state can be seen in Figures 32 and 33, respectively. The MC envelope of the MC signal is then extracted through quadrature demodulation. Subsequently, to determine the threshold limit and produce an error sample, the ACF of the signal is computed. CB-4 is released for 0.4 s with an additional delay to mimic islanding.

Figure 34 displays the VAMCE signal during tripping during this islanding case. The outcomes of this proposed method

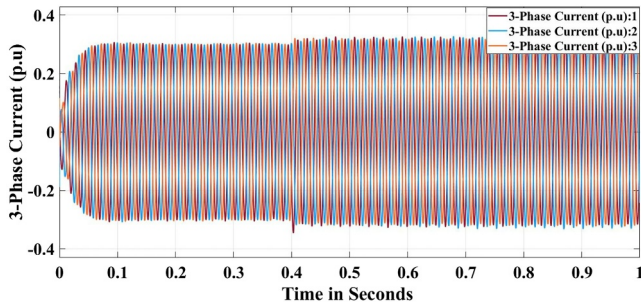


FIGURE 32 Case 4: 3-phase current signal in generation and load unbalanced condition.

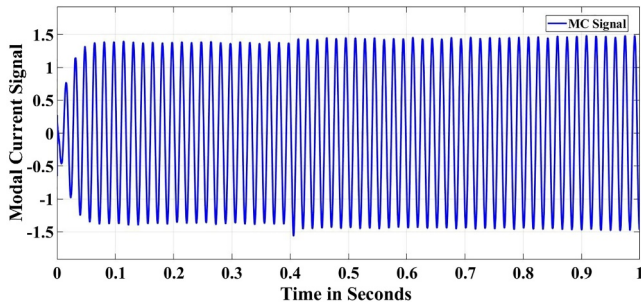


FIGURE 33 Case 4: MC signal in generation and load unbalanced condition.

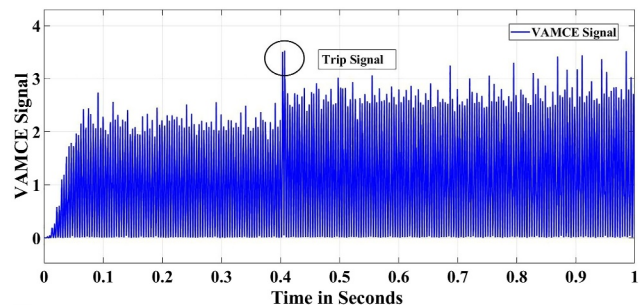


FIGURE 34 Case 4: VAMCE with trip signal in generation and load unbalanced condition.

demonstrate improved performance for different islanding scenarios and accurately identify the islanding at 0.4 s as compared to other envelope detection methods.

4 | DISCUSSION

The performance of some other techniques used in the literature has been compared with the results obtained in this paper. Other methods used in the literature are based on the ROCOF, O/UVP, O/UFP, and ROCOP. (a) The ROCOF (Rate of Change of Frequency) technique has a small NDZ and a detection time of 0.5 s. It does not impact power quality, is easy to implement, and is responsive to load switching. (b) The O/UVP (Under/Over Voltage Prevention) and O/UFP (Under/Over Frequency Prevention) techniques have large NDZ and a detection time of

0.2 s. It has no impact on power quality, and the disadvantage is the large NDZ. (c) The ROCOP (Rate of Change of Power) technique has a smaller NDZ than the OUVF/OUFP technique and its detection time is 24–26 milliseconds. It has no impact on power quality and is easy to implement. The disadvantage is that it fails to detect islanding when it is under a balanced load. Our proposed technique is also compared with passive islanding detection based on autocorrelation function on MC envelope signal for photovoltaic units. In ref. [43], the MC envelope signal is derived from the Hilbert transform and the duration needed to detect islanding is approximately 2–3 power frequency cycles, and the detection time is 0.5 s.

This paper uses the VAMCE technique to detect the islanding condition. This technique first monitors the current signal and transforms it into an MC signal. After this, The MC current signal's envelope is identified through the application of a demodulation technique. The performance of the four methods implemented in this paper is compared below; (a) The first case used for demodulation is synchronous real envelope detection, and the islanding detection time of this technique is 0.7 s. The drawback is that the difference in phase remains present in this instance. (b) The second case used for demodulation is the asynchronous complex square law method, and the identification duration of this technique to detect islanding is 0.6 s. (c) The third case used for demodulation is the square law method, and the detection time of this technique to detect islanding is 0.5 s. This technique is simple, but it can only demodulate low-level AM waves. (d) The fourth case used for demodulation is the quadrature demodulation method, and the detection duration of this technique to detect islanding is 0.4 s.

Hence, among all of the considered methods, the quadrature demodulation method quickly and precisely detects islanding conditions. The primary benefit of this approach is that, in this instance, the phase mismatch is erased.

The proposed VAMCE technique has a small NDZ and a few cycles of detection time. As discussed earlier, according to IEEE 1547-2003 [41, 42], IEEE 929-2000, and IEC-62116 standards, the maximum islanding time must not be more than 2 s. Here, the VAMCE technique along with the quadrature demodulation method quickly and precisely detects islanding conditions in just 0.4 s. When the islanding is detected, it operates protection relays which quickly activate circuit breakers and isolate the faulty microgrid from the healthy one. This rapid action ensures that the circuit breakers trip within islanding clearing time which in turn reduces the risk to equipment and improves power systems reliability. This method meets all practical requirements and additionally enhances the reliability and performance of islanding detection in distributed microgrid systems. It has high accuracy and reasonable speed of islanding detection under all conditions. It is also cost-effective; however, the implementation complexity is a bit high.

Table 2 shows the comparison of different demodulation techniques and their detection times. As can be seen from the table, the detection time is reduced from 0.7 to 0.4 s from synchronous real envelope detection to quadrature envelope detection, while the accuracy is increased from 50% to 98%.

TABLE 2 Comparison of different demodulation techniques.

Demodulation methods	Detection time (s)	Accuracy (%)
Synchronous real envelope detection	0.70	50
Asynchronous complex square law envelope detection	0.60	85
Square law envelope detection	0.50	90
Quadrature envelope detection	0.40	98

5 | CONCLUSIONS

This research offers an efficient passive islanding detection methodology that calculates the current signal at the PCC using the VAMCE technique. The method calculates the envelope of the signal using synchronous real demodulation, asynchronous complex square law demodulation, square law demodulation, and quadrature demodulation. Subsequently, it calculates the MC envelope signal's autocorrelation function, generating many samples. The VAMCE method can differentiate between islanding and non-islanding situations based on these samples. The efficacy of the suggested approach is illustrated by simulations conducted under various islanding and normal operational situations. The results reveal that the quadrature demodulation technique has high accuracy in detecting islanding conditions promptly, with a detection time of only 0.4 s and a low rate of NDZ. The system can be further improved in the future through the use of advanced artificial intelligence-based techniques to reduce detection time and NDZ.

AUTHOR CONTRIBUTION

Shanzah Naseem: Conceptualisation; data curation; formal analysis; software; visualisation; writing – original draft. **Sadiq Ahmad:** Conceptualisation; supervision; formal analysis; funding acquisition; methodology; project administration; resource; visualisation; writing – review editing. **Saddam Aziz:** Project administration; resource; visualisation; writing – review editing. **Muhammad Ali:** Methodology; project administration; resource. **Kazi N. Hasan:** Conceptualisation; formal analysis; funding acquisition; methodology; project administration; resource; visualisation; writing – review editing. **Ayaz Ahmad:** Conceptualisation; investigation; methodology; project administration; resources; supervision; writing – review editing. **Abdullah Shoukat:** Data curation; formal analysis; investigation; software; validation; visualisation; writing – review editing.

ACKNOWLEDGEMENT

Open access publishing facilitated by RMIT University, as part of the Wiley - RMIT University agreement via the Council of Australian University Librarians.

NOMENCLATURE

α, β, γ Modal variables
 \bar{x} Average

Φ	Phase difference
ACF	Auto correlation function
AFD	Active frequency drift
ANN	Artificial neural network
C_r	Carrier Amplitude
C_{lc}	Local carrier signal
CSI	Current source inverter
$DSB-TC$	Double side band transmitter carrier
DSB_{tc}	Double side band transmitter carrier
f_{cr}	Carrier frequency
FT	Fourier transform
g_I	Autocorrelation output
HHT	Hilbert hang transform
I	3-phase modal current signal
I_a, I_b, I_c	Pre-phase current measurements
$IDMs$	Islanding detection methods
$IIDG$	Inverter interface distributed generator
LPF	Low pass filter
MC	Modal current
MG	Microgrid
NDZ	Non detection zone
$P(t)$	In-phase component
PCC	Point of common coupling
PJD	Phase jump detection
PLC	Power line carrier communication
$PLCC$	Power line carrier communication
PNN	Probalistic neural network
$ROCOF$	Rate of change of frequency
$ROCOP$	Rate of change of output Power
$SCADA$	Supervisory control and data aquisition
SFS	Sandia frequency shift
SMS	Slip mode frequency shift
SMS	Slip mode frequency shifting
SNR	Signal to noise ratio
ST	Stockwell transform
SVM	Support vector machine
$T(t)$	Qadrature component
t	Time
THD	Total harmonic distortion
TTT	Time-time transform
$VAMCE$	Variance in auto correlation function of modal current
VSC	Voltage source converter
VU	Voltage unbalance
WPT	Wavelet packet transform
WT	Wavelet transform
x_j	j th sample signal value

CONFLICT OF INTEREST STATEMENT

The authors declare that there are no conflicts of interest.

DATA AVAILABILITY STATEMENT

The data supporting this study's findings are available from the corresponding author upon reasonable request.

ORCID

Kazi N. Hasan  <https://orcid.org/0000-0002-7315-5754>

REFERENCES

- Ang, T.Z., et al.: A comprehensive study of renewable energy sources: classifications, challenges and suggestions. *Energy Strategy Rev.* 43, 100939 (2022). <https://doi.org/10.1016/j.esr.2022.100939>
- Larik, N.A., et al.: A comprehensive literature review of conventional and modern islanding detection methods. *Energy Strategy Rev.* 44, 101007 (2022). <https://doi.org/10.1016/j.esr.2022.101007>
- Mumtaz, F., et al.: A Kalman filter-based protection strategy for microgrids. *IEEE Access* 10, 73243–73256 (2022). <https://doi.org/10.1109/access.2022.3190078>
- Naseem, S., et al.: Islanding detection in distributed microgrid using quadrature demodulation. In: 2022 International Conference on Technology and Policy in Energy and Electric Power (ICT-PEP), pp. 54–59. IEEE (2022)
- Reddy, C.R., et al.: Review of islanding detection parameters in smart grids. In: 2020 8th International Conference on Smart Grid (icSmart-Grid), pp. 78–89. IEEE (2020)
- Butt, I.Q., et al.: Passive islanding detection using square law method. In: 2021 International Conference on Emerging Power Technologies (ICEPT), pp. 1–6. IEEE (2021)
- Chowdhury, S.P., Chowdhury, S., Crossley, P.A.: Islanding protection of active distribution networks with renewable distributed generators: a comprehensive survey. *Electr. Power Syst. Res.* 79(6), 984–992 (2009). <https://doi.org/10.1016/j.epsr.2008.12.012>
- Namrata, K., Samadhiya, A., Ray, P.: A comprehensive review of active islanding detection methods and islanding assessment in a grid-connected solar-based microgrid. *Next-Gener. Smart Grids: Model., Control Optimiz.*, 153–180 (2022). https://doi.org/10.1007/978-981-16-7794-6_7
- Abo-Khalil, A.G., et al.: A modified active frequency islanding detection method based on load frequency and chopping fraction changes. *Int. Trans. Electr. Energy Syst.* 31(11), e13033 (2021). <https://doi.org/10.1002/2050-7038.13033>
- Vazquez, E., Vazquez, N., Femat, R.: Modified Sandia voltage shift anti-islanding scheme for distributed power generator systems. *IET Power Electron.* 13(18), 4226–4234 (2020). <https://doi.org/10.1049/iet-pel.2020.0735>
- Mrakić, D., Baghaee, H.R., Nikolovski, S.: Gibbs phenomenon-based hybrid islanding detection strategy for VSC-based microgrids using frequency shift, THD_U, and RMS_U. *IEEE Trans. Smart Grid* 10(5), 5479–5491 (2018). <https://doi.org/10.1109/tsg.2018.2883595>
- Baghaee, H.R., et al.: Anti-islanding protection of PV-based microgrids consisting of PHEVs using SVMs. *IEEE Trans. Smart Grid* 11(1), 483–500 (2019). <https://doi.org/10.1109/tsg.2019.2924290>
- Mukarram, M.J., Murkute, S.V.: Sandia frequency shift method for anti-islanding protection of a gridtied photovoltaic system. In: 2020 IEEE International Students' Conference on Electrical, Electronics and Computer Science (SCEECS), pp. 1–5. IEEE (2020, February)
- Jayanthi, S., Arockia Edwin Xavier, S., Manoharan, P.S.: Hybrid parametric islanding detection technique for microgrid system. *Bull. Pol. Acad. Sci. Tech. Sci.*, e140101 (2022). <https://doi.org/10.24425/bpasts.2022.140101>
- Guo, Z., et al.: An impedance identification-based islanding detection method for droop control inverters based on RDFT and positive-negative notch filters. *Energy Rep.* 8, 1060–1070 (2022). <https://doi.org/10.1016/j.egyr.2022.05.256>
- Yu, B.: Study on a correlation-based anti-islanding method under wider frequency trip settings for distributed generation. *Appl. Sci.* 10(10), 3626 (2020). <https://doi.org/10.3390/app10103626>
- Gupta, N., et al.: Review of islanding detection schemes for utility-interactive solar photovoltaic systems. *Int. J. Green Energy* 19(3), 242–253 (2022). <https://doi.org/10.1080/15435075.2021.1941048>
- Naraghipour, K., Ahmed, K., Booth, C.: A comprehensive review of islanding detection methods for distribution systems. In: 2020 9th International Conference on Renewable Energy Research and Application (ICRERA), pp. 428–433. IEEE (2020)
- Dubey, A.K., Mishra, J.P., Kumar, A.: Flexible distributed power converter with harmonic compensation and seamless passive islanding detection. In: 2020 IEEE International Conference on Power Electronics, Drives and Energy Systems (PEDES), pp. 1–6. IEEE (2020)
- Mahela, O.P., et al.: Islanding detection in utility grid with renewable energy using rate of change of frequency and signal processing technique. *AIMS Electron. Electr. Eng.* 6(2), 144–160 (2022). <https://doi.org/10.3934/electreng.2022009>
- Kulkarni, N.K., et al.: Reliable applicant for passive approach-based anti-islanding protection for different grid penetration levels of inverter-based distributed generation. In: 2022 International Conference for Advancement in Technology (ICONAT), pp. 1–6. IEEE (2022)
- Wang, G., et al.: Design consideration and performance analysis of a hybrid islanding detection method combining voltage unbalance/total harmonic distortion and bilateral reactive power variation. *CPSS Trans. Power Electron. Appl.* 5(1), 86–100 (2020). <https://doi.org/10.24295/cpsstpea.2020.00008>
- Mohanty, A., Rout, B., Pradhan, R.: A comparative Studies on different islanding detection methods for distributed generation systems. *Energy Sources, Part A Recovery, Util. Environ. Eff.* 45(1), 2284–2316 (2023). <https://doi.org/10.1080/15567036.2023.2186544>
- Bharti, I.P., et al.: Developments in islanding detection and its comparison: a comprehensive review. In: 2021 IEEE 8th Uttar Pradesh Section International Conference on Electrical, Electronics and Computer Engineering (UPCON), pp. 1–10. IEEE (2021)
- Mrakić, D., Baghaee, H.R., Nikolovski, S.: A novel ANFIS-based islanding detection for inverter-interfaced microgrids. *IEEE Trans. Smart Grid* 10(4), 4411–4424 (2018). <https://doi.org/10.1109/tsg.2018.2859360>
- Ashwin, K.V., et al.: A passive islanding detection technique based on susceptible power indices with zero non-detection zone using a hybrid technique. *Int. J. Intell. Syst. Appl. Eng.* 11(2), 635–647 (2023)
- Jhuma, U.K., Ahmad, S., Ahmed, T.: A novel approach for secure hybrid islanding detection considering the dynamic behavior of power and load in electrical distribution networks. *Sustainability* 14(19), 12821 (2022). <https://doi.org/10.3390/su141912821>
- Baghaee, H.R., et al.: Support vector machine-based islanding and grid fault detection in active distribution networks. *IEEE J. Emerg. Select. Top. Power Electron.* 8(3), 2385–2403 (2019). <https://doi.org/10.1109/jestpe.2019.2916621>
- Mohamad, H., et al.: Islanding detection based on rate of change of frequency over active power and PQ load insertion for synchronous distributed generation. In: 2022 IEEE International Conference in Power Engineering Application (ICPEA), pp. 1–6. IEEE (2022, March)
- Singh, S.K., et al.: A hybrid islanding detection technique for synchronous generator based microgrids. In: *Power Electronics and High Voltage in Smart Grid: Select Proceedings of SGESC 2021*, pp. 365–374. Springer Nature Singapore, Singapore (2022)
- Hariprasad, B., et al.: Island detection in inverter based distributed generation using a hybrid method. In: 2022 Second International Conference on Artificial Intelligence and Smart Energy (ICAIS), pp. 1702–1707. IEEE (2022, February)
- Larik, N.A., et al.: A comprehensive literature review of conventional and modern islanding detection methods. *Energy Strategy Rev.* 44, 101007 (2022). <https://doi.org/10.1016/j.esr.2022.101007>
- Nale, R., et al.: Real-time analysis of islanding detection scheme developed for AC microgrid system. *Elect. Power Syst. Res.* 226, 109926 (2024). <https://doi.org/10.1016/j.epsr.2023.109926>
- Lingampalli, B.R., et al.: Integrated microgrid islanding detection with phase angle difference for reduced nondetection zone. *Int. J. Energy Res.* 2023(1), 2275191–2275217 (2023). <https://doi.org/10.1155/2023/2275191>
- Hamed, N.A.H., Nyakoe, G.N., Saulo, M.J.: A hybrid islanding detection method based on Pearson correlation coefficient. *Int. J. Electr. Electron. Eng. Telecommun.*, 333–343 (2022). In press. <https://doi.org/10.18178/ijeetc.11.5.333-343>

36. Alex, R., Vinod, V., Shereef, R.M.: SVM-based anti-islanding protection for DER near a modern industrial premise. *Electr. Eng.* 105(1), 369–382 (2023). <https://doi.org/10.1007/s00202-022-01670-w>
37. Panchal, V., et al.: Comparative study of islanding detection techniques of microgrid for solar PV as distribution generator. In: *Intelligent Computing Techniques for Smart Energy Systems: Proceedings of ICTSES 2021*, pp. 635–648. Springer Nature Singapore, Singapore (2022)
38. Ghanbari, T., Farjah, E.: A multiagent-based fault-current limiting scheme for the microgrids. *IEEE Trans. Power Delivery* 29(2), 525–533 (2014). <https://doi.org/10.1109/tpwrd.2013.2282917>
39. Perera, N., Rajapakse, A.D., Buchholzer, T.E.: Isolation of faults in distribution networks with distributed generators. *IEEE Trans. Power Delivery* 23(4), 2347–2355 (2008). <https://doi.org/10.1109/tpwrd.2008.2002867>
40. IEEE recommended practice for utility interface of residential and intermediate photovoltaic (PV) systems, ANSI/IEEE Std 929-1988, p. 0 1, (1987)
41. IEEE 1547.1: IEEE Standard Conformance Test Procedures for Equipment Interconnecting Distributed Resources with Electric Power Systems (2005)
42. IEEE Standard 1547: IEEE Standard for Interconnecting Distributed Energy Resources with Electric Power System, 28 July, pp.1–16, (2003)
43. Haider, R., et al.: Passive islanding detection scheme based on autocorrelation function of modal current envelope for photovoltaic units. *IET Gener., Transm. Distrib.* 12(3), 726–736 (2018). <https://doi.org/10.1049/iet-gtd.2017.0823>

How to cite this article: Naseem, S., et al.: Intelligent islanding detection in smart microgrids. *IET Smart Grid.* 7(6), 1019–1035 (2024). <https://doi.org/10.1049/stg2.12197>